IEEE Access
Multidisciplinary | Rapid Review | Open Access Journal

Received May 28, 2021, accepted June 16, 2021, date of publication June 21, 2021, date of current version July 1, 2021.

Digital Object Identifier 10.1109/ACCESS.2021.3090814

Open-Circuit Fault Diagnosis of Six-Phase Permanent Magnet Synchronous Motor Drive System Based on Empirical Mode Decomposition Energy Entropy

YUE WU, ZHIFENG ZHANG, (Member, IEEE), YANG LI, AND QUANZENG SUN
School of Electrical Engineering, Shenyang University of Technology, Shenyang 110870, China

Corresponding author: Zhifeng Zhang (zzf_sut@126.com)

This work was supported by the National Natural Science Foundation of China "Study on fault diagnosis and fault-tolerant control of multi-phase motor drive control system for electric vehicle" under Grant 61603263.

ABSTRACT This paper proposes a method to diagnose the open-circuit faulty phases and faulty points of the six-phase permanent magnet synchronous motor (PMSM) drive circuit. The current sensor is used to obtain the six-phase current signal, and the least mean square error (LMS) adaptive filtering algorithm is used to filter out the vibration and noise. Empirical Mode Decomposition (EMD) is performed on the filtered current signals, and the EMD energy entropy of each phase current signal is calculated. The change of energy entropy can simplify the double-bridge arm open-circuit fault to the single-bridge arm open-circuit fault, which reduces the number of fault characteristics. After the faulty phase is judged by the change of energy entropy, the fault diagnosis system can diagnose the specific faulty point according to the normalized average value of each phase current signal. Finally, the current data of normal state and fault state are used to train the support vector machine (SVM) and classify the fault state. Each type of fault can be accurately diagnosed by substituting experimental data into the SVM. Experimental results prove that the proposed method can accurately diagnose the open-circuit faults of the six-phase PMSM drive system.

INDEX TERMS Six-phase permanent magnet synchronous motor, open-circuit fault, empirical mode decomposition, energy entropy, support vector machine.

I. INTRODUCTION

In recent years, multi-phase PMSM has been widely used in aircraft, electric vehicles, marine motor propulsion systems, and other important industrial fields requiring high reliability by the advantage of its low-voltage components to achieve high power, small torque ripple, and high fault tolerance [1]–[3]. Therefore, the research on optimal control, fault-tolerant control, and fault diagnosis of multi-phase PMSM has become a popular direction in the field of motor control [4]–[8]. Since the six-phase PMSM can still operate normally after a phase loss, an open-circuit fault will generate more harmonics, and the current distortion will cause the magnetic potential to change, which will cause more severe torque ripple and make the motor unstable. Therefore, it is significant to diagnose and identify the open-circuit faults of the single and double-bridge arm of the six-phase PMSM drive system. The safe and reliable operation of the motor can be guaranteed by obtaining the specific position of the open-circuit faulty point and cutting off the fault in time. At present, compared with the three-phase PMSM, there are fewer relevant kinds of literature on the open-circuit diagnosis of the six-phase PMSM drive. Because the six-phase PMSM has many parameters, complex conditions, and many considerations, it is necessary to propose a comprehensive diagnosis method that combines multiple methods [9]–[12].

The main faults of the six-phase PMSM drive circuit include short-circuit fault and open-circuit fault of IGBT. Compared with the open-circuit fault, the short-circuit fault occurs in an extraordinarily short time (usually about 10μs), and it is easy for the fault diagnosis system to diagnose open-circuit faults. In [13], a method of adding a fuse to the inverter circuit is proposed to convert the short-circuit fault of the inverter into an open-circuit fault. The advantage of

The associate editor coordinating the review of this manuscript and approving it for publication was Wei Xu.

this method is to improve the accuracy of fault diagnosis and make better use of topology reconstruction and fault tolerance measures. The diagnosis methods can be divided into voltage-based method and current-based method according to different fault characteristics. In [14]–[17], the voltage-based method is used for fault diagnosis.

The voltage-based method can be implemented with external hardware or model. In [18], the proposed method chooses a simple hardware circuit to replace the sensor to analyse the switch and judge the working state of the drive circuit, which requires a fast time to determine the faulty point, but its anti-interference performance is poor. In [19], the proposed method uses a voltage observer to estimate the actual output voltage of the converter, which reduces the false alarms. This method has good stability, but it is only suitable for high-performance drives.

In [20]–[24], the current-based method is used for fault diagnosis. The current-based method is used in most motor control, so it has the advantage of sharing a current sensor with the controller in the closed-loop system without the need for additional hardware. For example, it is used in field-oriented control and direct torque control. In [25], a method of fault diagnosis using reference current error is proposed, which uses the three-phase current and its corresponding reference signal to obtain the three-phase reference current error. Then the average value of the current error and the average absolute value of the motor phase current are used to realize the diagnostic variable. These variables are compared with defined thresholds to diagnose faults. However, it is difficult to determine the threshold when the load changes. In [26], a method of using the test phase current provided by the main control system as input is proposed, which avoids the use of additional sensors and prevents fault alarms. Moreover, the algorithm normalizes the current, so that it can define a general threshold that independent of the power and load of the motor.

In [27], the proposed method relies on the motor current signal, it uses a discrete wavelet transform to preprocess the three-phase output current and uses approximate coefficients to obtain the energy vector. Similar currents are compared by calculating the Euclidean distance between the energy vectors and diagnoses the faults. However, wavelets are easily affected by closed-loop systems. In [28], a method of using half-period phase difference current is proposed to diagnose multi-circuit faults of three-phase motors. This method only needs to collect phase currents to diagnose the multi-circuit points accurately, which improves the independence of diagnosis. In [29], a method of using EMD empirical mode to decompose entropy and extract dynamic feature information is proposed, which has high diagnostic accuracy.

This paper proposes a diagnosis method based on EMD energy entropy and normalized average current. When one or more phases in the drive circuit have open-circuit faults, the faulty phase entropy value will change significantly. The method is not affected by speed and torque, and the energy entropy value can reflect the degree of uniform change of signal. The advantage is that the double-bridge arm open-circuit fault is simplified to the single-phase bridge arm open-circuit fault. The calculation amount of the fault characteristic quantity is reduced, and the diagnosis is extraordinarily effective. Chapter 2 introduces the model of the six-phase PMSM drive system. Chapter 3 introduces the fault diagnosis method based on the EMD energy entropy and the normalized current method. The SVM is trained, and the fault state is classified and processed. Chapter 4 provides experimental results to verify the effectiveness of the proposed method. Chapter 5 summarizes the conclusions.

II. THE SIX-PHASE PMSM DRIVE SYSTEM MODEL

The main circuit topology of the six-phase voltage source inverter is shown in Fig.1, where U_{dc} is the DC voltage, T_1-T_{12} is the power switching device, and D_1-D_{12} is the anti-parallel diode. The input terminals of each phase are controlled by a pair of IGBT full bridge arms. Different voltage vectors are modulated by controlling the turn-on and turn-off time of the IGBT.

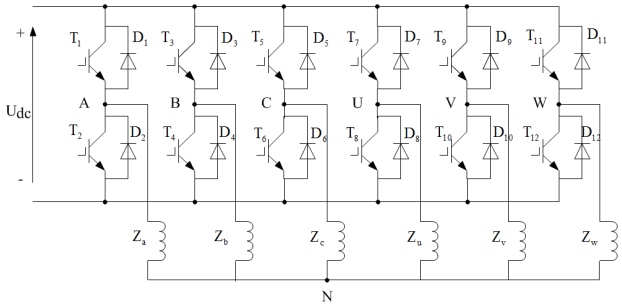

FIGURE 1. The main circuit topology of a six-phase voltage source inverter.

The open-circuit fault of the six-phase PMSM drive system can be divided into single-bridge arm open-circuit fault and double-bridge arm open-circuit fault. The number of single-bridge arm open-circuit faults in the six-phase PMSM drive system is 12. As shown in Fig.2(a), T_1 is open as an example. The number of double-bridge arm open-circuit faults in the six-phase PMSM drive system is 66. The double-bridge arm open-circuit faults can be divided into 3 types: the same side bridge arm of double-phase, the cross-side bridge arm of double-phase, the fully bridge arm of single-phase. The same side bridge arm of double-phase is shown in Fig.2(b), where both T_1 and T_3 are open as an example. The cross-side bridge arm of double-phase is shown in Fig.2(c), where both T_1 and T_4 are open as an example. The fully bridge arm of single-phase is shown in Fig.2(d), where both T_1 and T_2 are open as an example. Therefore, this paper analyzes 78 open-circuit faults and studies the diagnosis methods.

III. FAULT DIAGNOSIS OF THE DRIVE CIRCUIT

A. ELIMINATION OF MOTOR VIBRATION AND NOISE

In the six-phase PMSM drive system, the fault signal caused by the inverter open-circuit is often submerged by motor noise

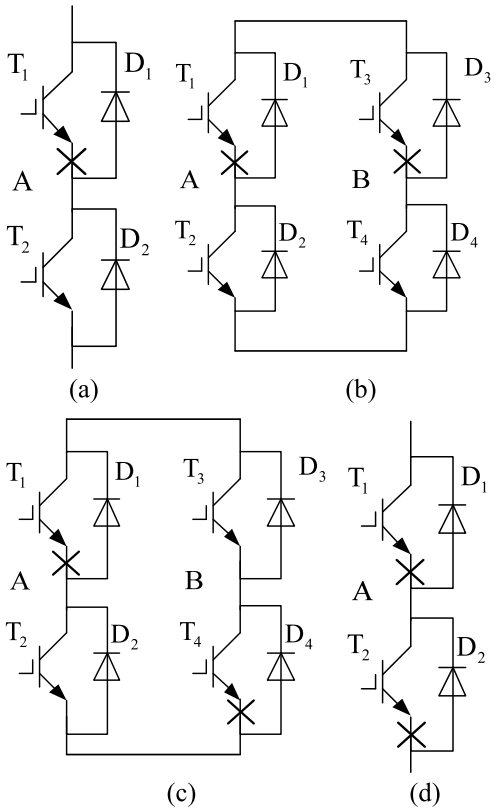

FIGURE 2. The open-circuit fault of the six-phase PMSM drive system.

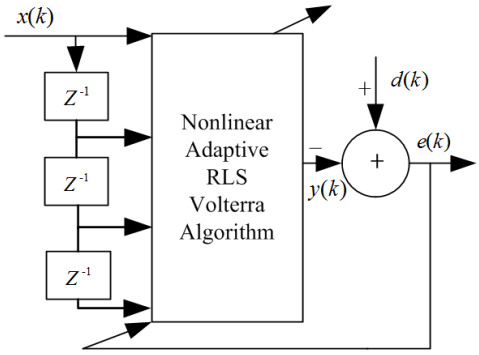

FIGURE 3. Basic structure of adaptive RLS volterra filter.

and environmental noise. The adaptive RLS Volterra filter is widely used in non-stationary and non-linear environments. It does not require prior knowledge of the original signal and noise pollution signal and has a certain adaptive adjustment ability. It has a good filtering effect to eliminate signal noise interference and environmental noise interference. The basic structure of the adaptive RLS Volterra filter is shown in Fig.3. x(k) is the current signal collected by the current sensor, d(k) is the set input signal, y(k) is the output signal of the adaptive algorithm, and e(k) is the output signal of the filter. The vibration and noise are set as the input signal. The deviation of d(k) and y(k) is the target function of the RLS Volterra algorithm [30], which is the equation (1).

When the objective function of the adaptive RLS Volterra algorithm is the smallest, the output is infinitely close to the set input motor vibration noise signal. The output signal of the filter is the current signal after eliminating the noise interference, which realizes the cancellation of the vibration and noise signal of the motor.

$$J = E\left\{|d(k) - y(k)|^2\right\} \tag{1}$$

B. DIAGNOSE FAULT PHASE BASED ON EMD ENERGY ENTROPY

When an open-circuit fault occurs in a multi-phase PMSM drive system, the characteristics vector formed by all fault features extracted has a large dimension and is difficult to be classified. Therefore, this paper introduces the entropy that can reflect the uniform distribution and uncertainty of the signal to diagnose the operating state of each phase. The EMD method is an adaptive signal processing method suitable for non-linear and non-stationary signals, and the EMD energy entropy can be obtained by introducing the definition of information entropy. The fault diagnosis method based on EMD energy entropy is selected to diagnose the open-circuit faulty phase of the six-phase PMSM system. The six-phase current signal $I_i(t)$ collected by the current sensor is analyzed by EMD method, and many IMF components with different frequency bands $c_j(t)$ and a margin $r_n(t)$ are obtained. The current signals of the A-phase open-circuit fault and normal state on the upper bridge arm are taken as an example. The first four IMF components obtained by EMD method for the current signal are shown in Fig.4.

For each IMF component [31] $c_j(t)$ is calculated by the equation (2).

$$E_j = \int_{-\infty}^{+\infty} |c_j(t)|^2 dt \tag{2}$$

E_j is the energy of each component of IMF. The obtained E_j is calculated by the equation (3).

$$p_j = E_j / \sum_{j=1}^{n} E_j \tag{3}$$

The percentage of E_j in the total energy of the signal is p_j. The equation (4) is used to calculate the obtained p_j [32].

$$H_{EN} = -\sum_{j=1}^{n} p_j \log_2 p_j \tag{4}$$

The EMD energy entropy H_{EN} of the six-phase current signal can be obtained.

It can be seen from Fig.4 that the distribution uniformity of the current signal is different under fault state and normal state, so the EMD entropy value is also different. The energy entropy of EMD in fault state changes obviously. The examples of diagnosing single-bridge arm open-circuit fault of inverter and double-bridge arm open-circuit of the inverter are listed to verify the effectiveness of the diagnosis method. The motor operating conditions are set as the speed of 100 rad/s

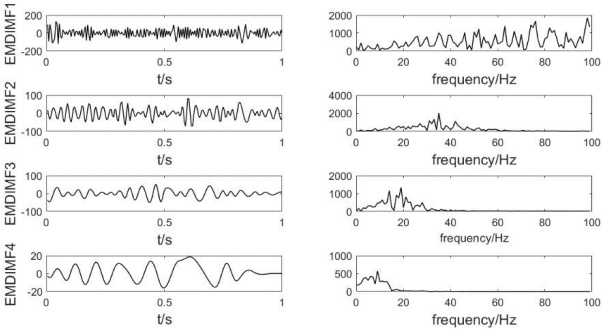

FIGURE 4. A-phase current IMF component diagram.

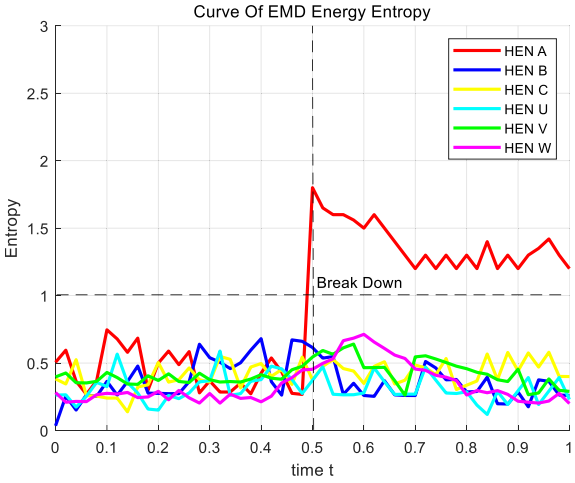

FIGURE 5. Curve of current entropy when the upper bridge arm of A-phase is opened.

and the torques of 50Nm, and the fault is set at 0.5s. The curve of entropy value changing with time can be obtained by the sliding window method, with the window length set to the sampling frequency and the sliding speed set to 1. The following four examples of faults illustrate the changes in entropy, which are the open-circuit faults that occur in the single-bridge arm of single-phase, the same side the bridge arm of double-phase, the cross side of the bridge arm in double-phase, the full-bridge arm of single-phase.

Entropy changes during four types of faults: (1) Single-phase single-bridge open-circuit taking the A-phase upper bridge arm open-circuit as an example, the six-phase current EMD energy entropy curve is shown in Fig.5, and the red curve shows the change of entropy of A-phase. It can be seen from the figure that the EMD energy entropy value of the faulty phase current increases rapidly near the 0.5s faulty point and exceeds 1, while the non-faulty phase entropy value has little effect, and there is no obvious sudden change. The entropy value is always below 1, and there is a clear difference between the EMD energy entropy of the faulty phase and the non-faulty phase.

(2) Open-circuit fault occurs in the same side bridge arm of double-phase, that is, the double-phase upper bridge arm or lower bridge arm has an open-circuit fault at the same time. The fault takes the A-phase upper bridge arm and

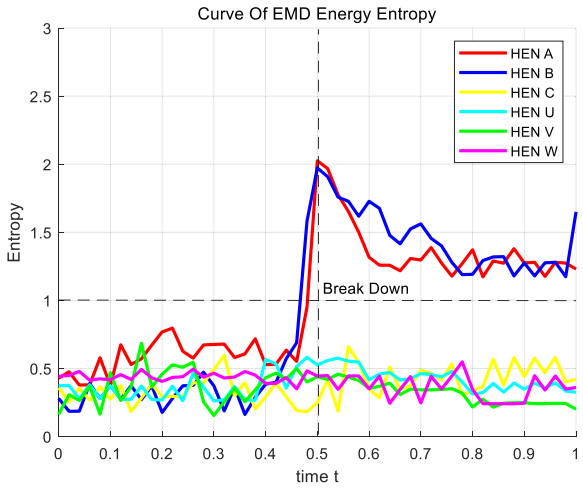

FIGURE 6. Curve of current entropy when the upper bridge arm of A-phase and B-phase is opened.

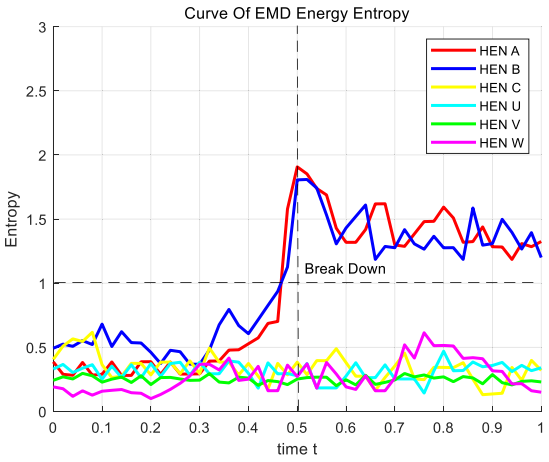

FIGURE 7. Curve of current entropy when the upper bridge arm of A-phase and lower bridge arm of B-phase is opened.

the B-phase upper bridge arm have an open-circuit fault as examples. The six-phase current EMD energy entropy change curve is shown in Fig.6. The red curve shows the change of entropy of the A-phase, and the blue curve shows the change of entropy of the B-phase. It can be seen from Fig.6 that when the drive system occurs the fault, entropy value of the faulty phase is greater than 1, and the EMD energy entropy value of the non-faulty phase is less than 1 most of the time.

(3) Open-circuit fault occurs in the cross side of the bridge arm of double-phase. Take the A-phase upper bridge arm open-circuit fault and the B-phase lower bridge arm open-circuit fault as an example. The entropy curve is shown in Fig.7 below, and the red curve shows the change of entropy of the A-phase, and the blue curve shows the change of entropy of the B-phase. It can be seen from Fig.7 that the change of phase entropy value of the cross side of the double-bridge arm open-circuit fault is the same as that of a single-bridge arm open-circuit fault. The non-faulty phase entropy is less than 1 most of the time, and the faulty phase entropy will be greater than 1.

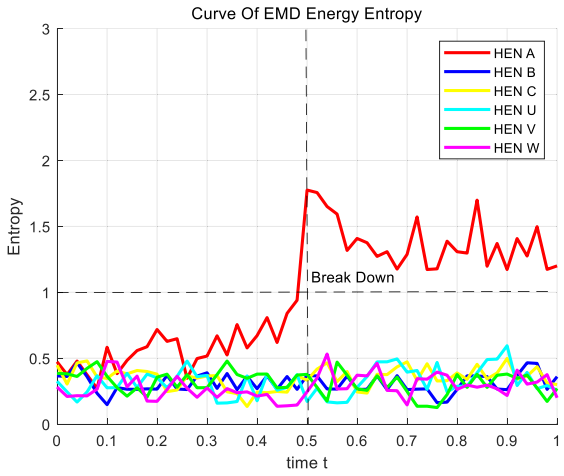

FIGURE 8. Curve of current entropy when the upper and lower bridge arm of A-phase is opened.

(4) Open-circuit fault occurs in fully bridge arm of the single-phase. Take the A-phase fully bridge arm open-circuit as an example, and the entropy curve is shown in Fig.8. The red curve shows the change of entropy of A-phase, at 0.5s when the upper and lower bridge arms of A-phase have an open-circuit fault at the same time, the A-phase current value is 0, and the entropy value is about 1. It can be seen from Fig.8 that the entropy value of the non-faulty phase is not affected by the full-bridge arm of the faulty phase, and the current entropy value of the non-faulty phase is always less than 1.

According to the analysis of Fig.5-8, when the inverter has an open-circuit fault, the entropy value of the faulty phase current will increase, and it is significantly greater than that of the non-faulty phase, while the entropy value of the non-faulty phase will change between 0 and 1.

The EMD energy entropy of the faulty phase changes greater than 1, while the EMD energy entropy of the non-faulty phase changes in the range of 1 and 0, so the energy entropy threshold is set to 1. Thus, the double-bridge arm of double-phase open-circuit fault can be transformed into the combination of two single-bridge arms of single-phase open-circuit faults. Because the entropy cannot diagnose the specific location of the faulty point, the next chapter uses the normalized average current method to improve the fault diagnosis process.

C. THE NORMALIZED AVERAGE CURRENT METHOD FOR ACCURATE JUDGMENT OF THE FAULTY POINT

In the previous section, the faulty phase and the non-faulty phase have been judged by the entropy value. This section conducts fault diagnosis on the specific point of the open-circuit bridge arm of the faulty phase of the six-phase PMSM inverter. Using the normalized average current method [33], the specific process is:

(1) Calculate the average value of the six-phase current i_n, n=A,B,C,U,V,W.

$$\bar{I}_n = \frac{\omega_s}{2\pi}\int_0^{\frac{\omega_s}{2\pi}} i_n dt \tag{5}$$

Among them, $\bar{I}_n$ is the average current per phase of the stator winding of the PMSM, and ω_s is the angular velocity of the PMSM.

(2) Calculate the absolute value of the six-phase current i_n, and then use equation (5) to calculate the absolute average current value $|\bar{I}_n|$, $n = A, B, C, U, V, W$.

(3) Use the absolute average current value $\bar{I}_n$ to normalize the average current $\bar{I}_n$ in equation (5) to obtain the normalized average value $\bar{I}_{nN}$, $n = A, B, C, U, V, W$.

$$\bar{I}_{nN} = \frac{\bar{I}_n}{|\bar{I}_n|} \tag{6}$$

The $\bar{I}_{nN}$ is compared to the threshold value δ. If $\bar{I}_{nN} > \delta$, the lower bridge arm of the phase appears open-circuit fault, if $\bar{I}_{nN} < -\delta$, the upper bridge arm of the phase appears open-circuit fault. The fault diagnosis table is shown in Table 1.

TABLE 1. Fault diagnosis list.

Switch	$\bar{I}_{AN}$	$\bar{I}_{BN}$	$\bar{I}_{CN}$	$\bar{I}_{UN}$	$\bar{I}_{VN}$	$\bar{I}_{WN}$
T1	<-δ					
T2	>δ					
T3		<-δ				
T4		>δ				
T5			<-δ			
T6			>δ			
T7				<-δ		
T8				>δ		
T9					<-δ	
T10					>δ	
T11						<-δ
T12						>δ

When the inverter is operating normally, $\bar{I}_{nN}$ is equal to 0. When an open-circuit fault occurs in the single-bridge arm, $\bar{I}_{nN}$ is close to ± 1, and it can be concluded that the threshold should be greater than 0 and less than 1. The threshold can be able to adapt to the current transient during normal operation, and no faulty alarms will occur. The normalized average current value is close to ± 1, when the actual inverter has a single-bridge arm open-circuit fault, this paper sets the δ to 0.45 according to [34].

D. DIAGNOSE FAULT STATES BASED ON SVM

The problem of the single-bridge arm and double-bridge arm open-circuit fault diagnosis in the six-phase PMSM drive

TABLE 2. The fault state output comparison.

A+	B+	C+	U+	V+	W+
211111	121111	112111	111211	1111211	111112
A-	B-	C-	U-	V-	W-
311111	131111	113111	111311	1111311	111113
A+ B+	A+ C+	A+ U+	A+ V+	A+ W+	V+W+
221111	212111	211211	211121	211112	111122
A- B-	A-C-	A- U-	A- V-	A-W-	V-W-
331111	313111	311311	311131	311113	111133
B+C+	B+U+	B+V+	B+W+	U+V+	U+W+
122111	121211	121121	121112	111221	111212
B-C-	B-U-	B-V-	B-W-	U-V-	U-W-
133111	131311	131131	131113	111331	111313
C+U+	C+V+	C+W+	C-U-	C-V-	C-W-
112211	112121	112112	113311	113131	113113
A+ B-	A+ C-	A+ U-	A+ V-	A+ W-	V+W-
231111	213111	211311	211131	211113	111123
A- B+	A- C+	A- U+	A- V+	A- W+	V-W+
321111	312111	311211	311121	311112	111132
B+C-	B+U-	B+V-	B+W-	U+V-	U+W-
123111	121311	121131	121113	111231	111213
B-C+	B-U+	B-V+	B-W+	U-V+	U-W+
132111	131211	131121	131112	111321	111312
C+U-	C+V-	C+W-	C-U+	C-V+	C-W+
112311	112131	112113	113211	113121	113112
A+A-	B+B-	C+C-	U+U-	V+V-	W+W-
411111	141111	114111	111411	1111411	111114

system is simplified to the single-phase open-circuit fault. The SVM with a better classification effect of small samples is used to diagnose the fault state of each phase, and the indirect classification method is used to construct a one-to-many SVM classifier, and 4 SVM sub-classifiers are set to correspond to these 4 operating states. The six-phase current EMD energy entropy value and the normalized average current are taken as the fault characteristic value as shown in equation (7).

$$T = \begin{bmatrix} H_{ENA} & \bar{I}_{AN} \\ H_{ENB} & \bar{I}_{BN} \\ H_{ENC} & \bar{I}_{CN} \\ H_{ENU} & \bar{I}_{UN} \\ H_{ENV} & \bar{I}_{VN} \\ H_{ENW} & \bar{I}_{WN} \end{bmatrix} \tag{7}$$

The operating state of each phase SVM should output six-dimensional parameters and set the output value of each phase to 1, 2, 3, 4, respectively with normal operation, upper bridge arm open-circuit fault, lower bridge arm open-circuit fault, and fully bridge arm open-circuit fault. In the six-phase PMSM drive system, the inverter has a total of 78 fault states for single-bridge arm and double-bridge arm open-circuit faults. The open-circuit fault of the upper bridge arm is set to "+", and the open-circuit fault of the lower bridge arm is set to "−". Table 2 shows the correspondence between 78 fault states and the output labels of the SVM classifier.

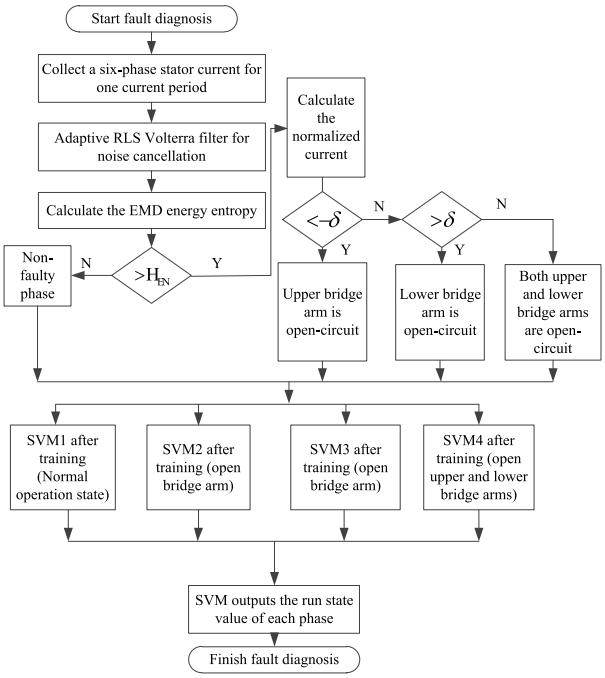

FIGURE 9. Flow chart of diagnosis plan.

In order to clearly understand the fault diagnosis method, the flow chart is shown in Fig.9. First, the LMS adaptive algorithm is used to calculate the EMD energy entropy of the filtered current, and the energy entropy threshold H_{EN} is set. If the EMD energy entropy value of a certain phase is greater than the entropy threshold H_{EN}, the bridge arm has an open-circuit fault, and fault diagnosis will continue; if the EMD energy entropy value of a certain phase is less than or equal to the entropy threshold H_{EN}, the bridge arm is normal operation. Here the threshold A is set to 1.

Then the normalized average current of the six-phase stator current values is calculated, the normalized average current thresholds δ and $-\delta$ are set, when the normalized average value of a certain phase current is less than the threshold $-\delta$, the upper bridge arm has an open circuit fault. If the normalized average value of a certain phase current is greater than the threshold δ, the lower bridge arm has an open-circuit fault. The value of δ is 0.45.

Finally, the six-phase current entropy value and the normalized current value are input into the four SVM sub- classifiers as fault characteristic values. The SVM sub-classifier has output values of 1, 2, 3, and 4 for the four operating states of normal operation, upper bridge arm open-circuit fault, lower bridge arm open-circuit fault, and fully bridge arm open-circuit fault. Through the look-up table method, the specific open-circuit location point of the inverter can be accurately diagnosed.

IV. EXPERIMENTAL RESULTS

The experimental platform of the six-phase PMSM is shown in Fig.10. The main experimental equipment includes the inverter, microcontroller, oscilloscope, microcontroller

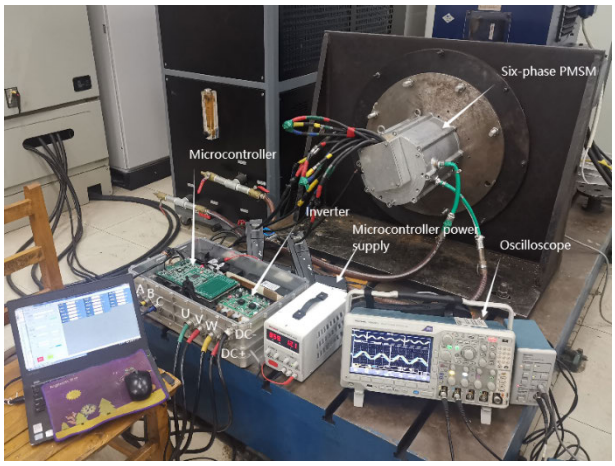

FIGURE 10. Six-phase PMSM system experiment platform.

power supply, six-phase PMSM. The cooling method of the motor is water-cooled. The actual fault current parameter value is obtained through the experimental platform. The calculation program of EMD energy entropy and normalized average current is completed by using mathematical software.

Set the speed of 100 rad/s, the torque of 50 Nm; the speed of 130 rad/s, the torque of 50 Nm; the speed of 130 rad/s, the torque of 60 Nm operating conditions. Set the six-phase PMSM drive system normal operation, the upper bridge arm open-circuit fault, lower bridge arm open-circuit fault, and fully bridge arm open-circuit fault, these four operating states. Under the operating conditions of the speed of 100 rad /s, the torque of 50 Nm and the speed of 130 rad/s, the torque of 50 Nm, the current values of four operating states are collected.

The collected current signal is continuously intercepted for a current cycle length until the end of the system operation. A total of 100 groups of six-phase current signals are intercepted in each operation state. EMD energy entropy and the normalized average current value of each six-phase current signal under each operation state are calculated. Each operation state takes 100 groups to form 400 groups of fault feature vectors. 400 sets of fault feature vectors are used as SVM training data, so there are a total of 4800 training data.

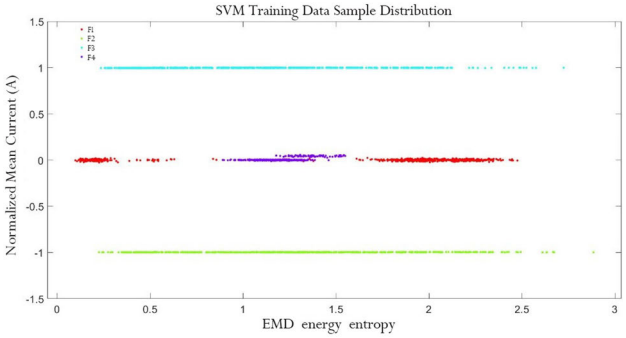

FIGURE 11. Training data sample distribution.

The distribution of training data samples is shown in Fig.11. The characteristics vectors of tags F1, F2, F3,

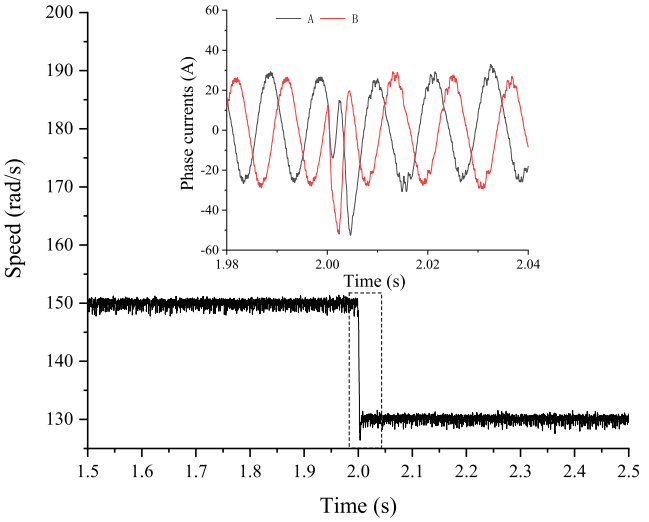

FIGURE 12. The speed and current of normal operation.

and F4 respectively indicate normal operation, the upper bridge arm open-circuit fault, lower bridge arm open-circuit fault, and fully bridge arm open-circuit fault. Each type of characteristics vector in the figure has good aggregation, and each type of characteristics vector can be distinguished. In order to test the accuracy of the fault diagnosis system, four kinds of fault experiments are carried out under the working conditions of 130 rad/s and 60 Nm, and the normal operation experiment of changing the speed is carried out. The actual classification and prediction classification of test data and the accuracy of fault diagnosis are as follows: (T_1 T_2 T_3 T_4 is shown in Fig.1).

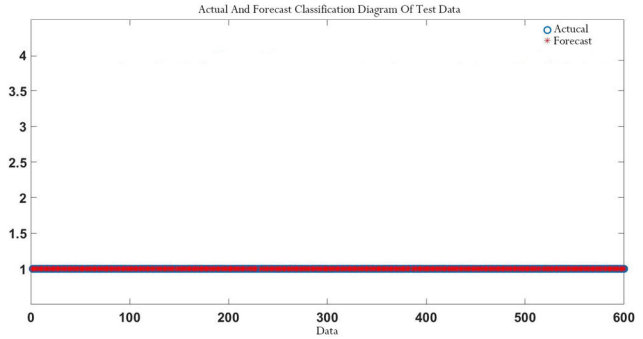

FIGURE 13. Actual and forecast classification diagram of normal operation.

A. THE NORMAL OPERATION: NO OPEN-CIRCUIT FAULT OCCURS IN THE INVERTER

The speed and current of normal operation are shown in Fig.12. After stable operation for 2s, the speed drops from 150 rad/s to 130 rad/s and the current also decreases. The actual classification diagram and forecast classification diagram of normal operation are shown in Fig.13. The blue circle represents the test set for actual classification, and the red

asterisk indicates the test set for forecast classification. When the blue circle overlaps the red asterisk, the fault diagnosis is accurate. There is no misjudgment point in Fig.13, which proves that the fault diagnosis method will not be affected when the motor changes its operating conditions during normal operation.

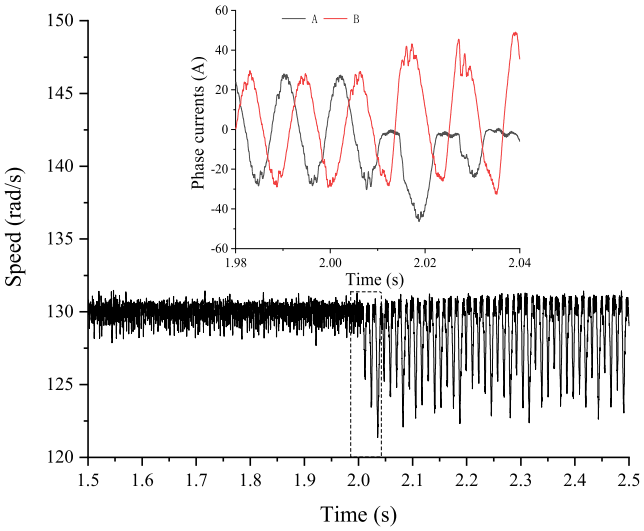

FIGURE 14. The speed and current of fault type I.

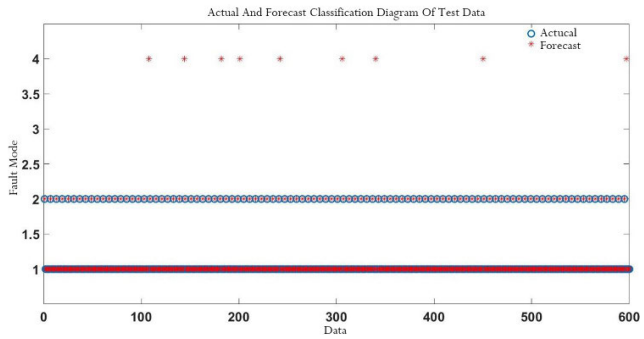

FIGURE 15. Actual and forecast classification diagram of fault type I.

B. THE FAULT TYPE I: OPEN-CIRCUIT FAULT OCCURS IN THE SINGLE-BRIDGE ARM OF SINGLE-PHASE

The fault type I is that the upper bridge arm T_1 of A-phase in the inverter is open-circuit. According to the designed SVM classifier, the output value is 211111. The output value of A-phase is 2, which indicates that the upper bridge arm has an open-circuit fault. The output value of other phases is 1, which indicates normal operation. The speed and current of the fault type I are shown in Fig.14. After stable operation for 2s, the A-phase upper bridge arm has an open-circuit fault, so only the current waveform of the lower bridge arm is displayed, and the speed fluctuates significantly. The actual classification diagram and forecast classification diagram of the fault type I are shown in Fig.15. There are 9 misjudgment points in 600 test data, and the misjudgment points are diagnosed as the fault type IV.

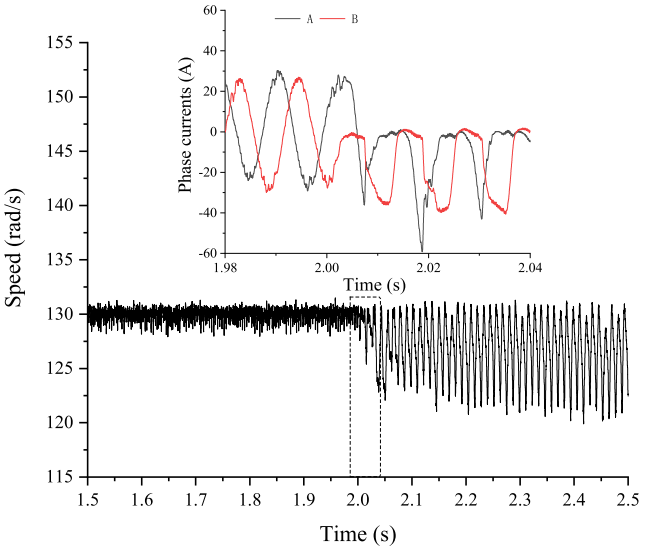

FIGURE 16. The speed and current of fault type II.

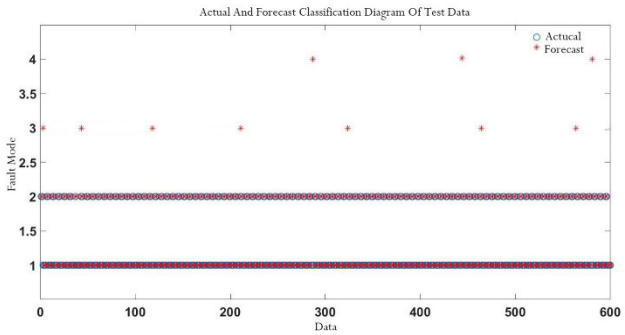

FIGURE 17. Actual and forecast classification diagram of fault type II.

C. THE FAULT TYPE II: OPEN-CIRCUIT FAULT OCCURS IN THE SAME SIDE BRIDGE ARM OF DOUBLE-PHASE

The fault type II is that the upper bridge arm T_1 of A-phase and the upper bridge arm T_3 of B-phase are open-circuit. According to the designed SVM classifier, the output value is 221111. The speed and current of the fault type II are shown in Fig.16. After stable operation for 2s, the A-phase upper bridge arm and B-phase upper bridge arm have an open-circuit fault. Therefore the current waveforms of A-phase lower bridge arm and B-phase lower bridge arm are displayed, and the speed fluctuation is more obvious. The actual classification diagram and forecast classification diagram of the fault type II are shown in Fig.17. There are 10 misjudgment points in 600 test data. Most of misjudgment points are diagnosed as the fault type III, and a few misjudgment points are diagnosed as the fault type IV.

D. THE FAULT TYPE III: OPEN-CIRCUIT FAULT OCCURS IN THE CROSS SIDE BRIDGE ARM OF DOUBLE-PHASE

The fault type III is that the upper bridge arm T_1 of A-phase and the lower bridge arm T_4 of B-phase are open-circuit. According to the designed SVM classifier, the output value

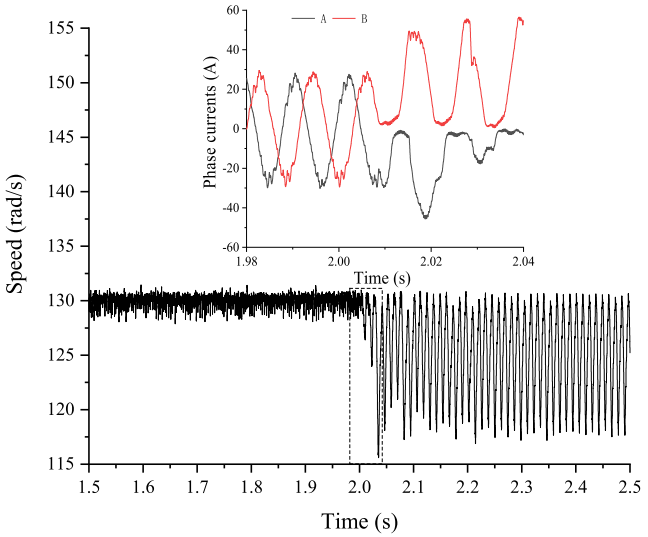

FIGURE 18. The speed and current of fault type III.

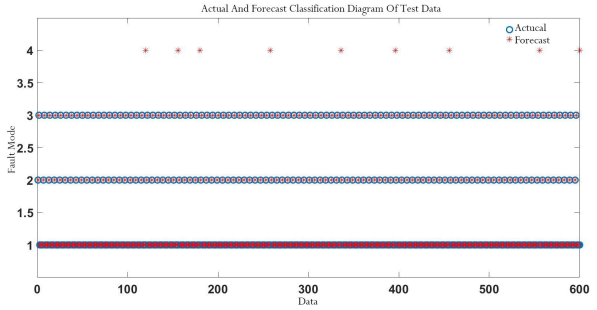

FIGURE 19. Actual and forecast classification diagram of the fault type III.

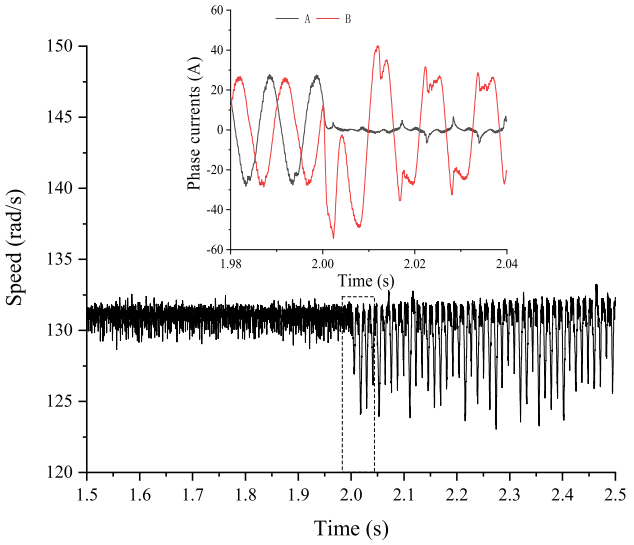

FIGURE 20. The speed and current of fault type IV.

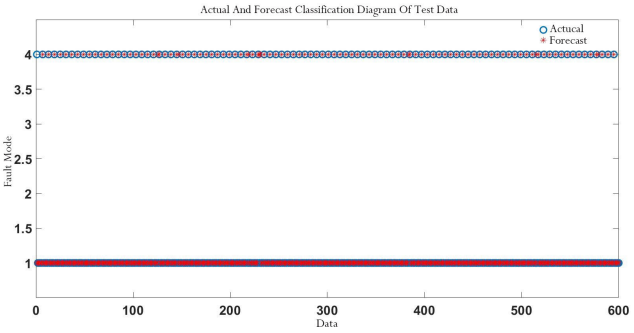

FIGURE 21. Actual and forecast classification diagram of fault type IV.

is 231111. The output value of B-phase is 3, which indicates that the lower bridge arm has an open-circuit fault. The speed and current of the fault type III are shown in Fig.18. After stable operation for 2s, the A-phase upper bridge arm and B-phase lower bridge arm have an open-circuit fault. Therefore the current waveforms of A-phase lower bridge arm and B-phase upper bridge arm are displayed, and the speed fluctuation is similar to the fault type II. The actual classification diagram and forecast classification diagram of the fault type III is shown in Fig.19. There are 9 misjudgment points in 600 test data, and the misjudgment points are diagnosed as the fault type IV.

E. THE FAULT TYPE IV: OPEN-CIRCUIT FAULT OCCURS IN THE DOUBLE-BRIDGE ARM OF THE SINGLE-PHASE

The fault type IV is that the upper bridge arm T_1 and the lower bridge arm T_2 of A-phase are open-circuit. According to the designed SVM classifier, the output value is 411111. The output value of A-phase is 4, which indicates that the fully bridge arm has an open-circuit fault.

The speed and current of the fault type IV are shown in Fig.20. After stable operation for 2s, the A-phase fully bridge arm has an open-circuit fault. Therefore, the current of A-phase is close to zero. The actual classification diagram and forecast classification diagram of the fault type IV is shown in Fig.21. There are 7 misjudgment points in 600 test data.

TABLE 3. Fault diagnosis accuracy table.

Fault state	Number of correct diagnoses	Number of test samples	Judging accuracy
No fault	600	600	100%
A+	591	600	98.5%
A+B+	590	600	98.3%
A+B-	591	600	98.5%
A+A-	593	600	98.8%

Table 3 shows the accuracy of the diagnostic method. It can be seen from Fig.12-21 and Table 3 that the fault diagnosis method is effective for test data. The SVM classifier is composed of the EMD energy entropy and the normalized average current. The specific conditions of the SVM classification of the test data and the accuracy of the fault diagnosis show that the fault vector has a superb classification effect and the classifier output can accurately diagnose the faulty point.

V. CONCLUSION

In order to diagnose the open-circuit fault of the six-phase PMSM drive circuit, a new fault diagnosis method is proposed. Firstly, the EMD energy entropy of the current is calculated by LMS adaptive filtering algorithm, and the energy entropy of the faulty phase change obviously, so the non-faulty phase and faulty phase can be distinguished. Secondly, the normalized average current of the six-phase stator current is calculated, and the specific faulty point is judged. Finally, the entropy value of the six-phase current and the normalized average current value are input into the four SVM sub-classifiers as fault characteristics. SVM sub-classifier classifies the normal operation, upper bridge arm open-circuit fault, lower bridge arm open-circuit fault, and fully bridge arm open-circuit fault. The faulty phase and faulty point of open-circuit can be distinguished according to the state table.

Compared with other fault diagnosis methods, this method has some unique advantages.

(1) The diagnosis method combining LMS adaptive filtering and EMD energy entropy has strong anti-noise ability, which can effectively offset the interference of motor vibration and noise when collecting current signal, and the fault characteristic are more obvious.
(2) The energy entropy is not affected by the torque and speed and can well reflect the internal uniform change degree of the signal, which effectively solves the problem that the fault characteristics quantity is easily affected by the load change. The accuracy of fault diagnosis is improved.
(3) The double-bridge arm of double-phase open-circuit fault of the six-phase PMSM drive system is simplified as a single-phase bridge arm open-circuit fault, which reduces the calculation of fault characteristics and improves the efficiency of fault diagnosis.

This means that an accurate fault diagnosis method is provided for the open-circuit fault of the six-phase PMSM drive system. And new ideas and references are provided for the open-circuit fault diagnosis method of multi-phase PMSM drive system.

REFERENCES

[1] X. Wang, Z. Wang, Z. Xu, M. Cheng, W. Wang, and Y. Hu, "Comprehensive diagnosis and tolerance strategies for electrical faults and sensor faults in dual three-phase PMSM drives," *IEEE Trans. Power Electron.*, vol. 34, no. 7, pp. 6669–6684, Jul. 2019.
[2] A. Arafat, S. Choi, and J. Baek, "Open-phase fault detection of a five-phase permanent magnet assisted synchronous reluctance motor based on symmetrical components theory," *IEEE Trans. Ind. Electron.*, vol. 64, no. 8, pp. 6465–6474, Aug. 2017.
[3] A. Hezzi, S. B. Elghali, Y. B. Salem, and M. N. Abdelkrim, "Control of five-phase PMSM for electric vehicle application," in *Proc. 18th Int. Conf. Sci. Techn. Autom. Control Comput. Eng. (STA)*, Dec. 2017, pp. 205–211.
[4] H. Lin, H. Guo, and H. Qian, "Design of high-performance permanent magnet synchronous motor for electric aircraft propulsion," in *Proc. 21st Int. Conf. Electr. Mach. Syst. (ICEMS)*, Oct. 2018, pp. 174–179.
[5] X. Kuang, H. Guo, J. Xu, and T. Zhou, "Research on a six-phase permanent magnet synchronous motor system at dual-redundant and fault tolerant modes in aviation application," *Chin. J. Aeronaut.*, vol. 30, no. 4, pp. 1548–1560, Aug. 2017.
[6] W. Huang, W. Hua, F. Chen, and J. Zhu, "Enhanced model predictive torque control of fault-tolerant five-phase permanent magnet synchronous motor with harmonic restraint and voltage preselection," *IEEE Trans. Ind. Electron.*, vol. 67, no. 8, pp. 6259–6269, Aug. 2020.
[7] S. F. Toloue, S. H. Kamali, and M. Moallem, "Torque ripple minimization and control of a permanent magnet synchronous motor using multiobjective extremum seeking," *IEEE/ASME Trans. Mechatronics*, vol. 24, no. 5, pp. 2151–2160, Oct. 2019.
[8] X. Zhou, J. Sun, H. Li, M. Lu, and F. Zeng, "PMSM open-phase fault-tolerant control strategy based on four-leg inverter," *IEEE Trans. Power Electron.*, vol. 35, no. 3, pp. 2799–2808, Mar. 2020.
[9] Z. Zhang, Y. Wu, and S. Qi, "Diagnosis method for open-circuit faults of six-phase permanent magnet synchronous motor drive system," *IET Power Electron.*, vol. 13, no. 15, pp. 3305–3313, Nov. 2020.
[10] H. Guo, S. Guo, J. Xu, and X. Tian, "Power switch open-circuit fault diagnosis of six-phase fault tolerant permanent magnet synchronous motor system under normal and fault-tolerant operation conditions using the average current Park's vector approach," *IEEE Trans. Power Electron.*, vol. 36, no. 3, pp. 2641–2660, Mar. 2021.
[11] Z. Jian-Jian, C. Yong, C. Zhang-Yong, and Z. Anjian, "Open-switch fault diagnosis method in voltage-source inverters based on phase currents," *IEEE Access*, vol. 7, pp. 63619–63625, 2019.
[12] M. Breznik, V. Ambrožič, and M. Nemec, "Detection of open circuit fault in battery power supply feeding permanent magnet synchronous motor," *IET Power Electron.*, vol. 11, no. 14, pp. 2377–2384, Nov. 2018.
[13] V. F. M. B. Melo, C. B. Jacobina, and N. Rocha, "Fault tolerance performance of dual-inverter-based six-phase drive system under single-, two-, and three-phase open-circuit fault operation," *IET Power Electron.*, vol. 11, no. 1, pp. 212–220, Jan. 2018.
[14] S. Karimi, P. Poure, and S. Saadate, "Fast power switch failure detection for fault tolerant voltage source inverters using FPGA," *IET Power Electron.*, vol. 2, no. 4, pp. 346–354, Jul. 2009.
[15] C. Shu, C. Ya-Ting, Y. Tian-Jian, and W. Xun, "A novel diagnostic technique for open-circuited faults of inverters based on output line-to-line voltage model," *IEEE Trans. Ind. Electron.*, vol. 63, no. 7, pp. 4412–4421, Jul. 2016.
[16] Z. Li, H. Ma, Z. Bai, Y. Wang, and B. Wang, "Fast transistor open-circuit faults diagnosis in grid-tied three-phase VSIs based on average bridge arm pole-to-pole voltages and error-adaptive thresholds," *IEEE Trans. Power Electron.*, vol. 33, no. 9, pp. 8040–8051, Sep. 2018.
[17] M. A. Rodriguez-Blanco, A. Vazquez-Perez, L. Hernandez-Gonzalez, V. Golikov, J. Aguayo-Alquicira, and M. May-Alarcon, "Fault detection for IGBT using adaptive thresholds during the turn-on transient," *IEEE Trans. Ind. Electron.*, vol. 62, no. 3, pp. 1975–1983, Mar. 2015.
[18] Q.-T. An, L.-Z. Sun, K. Zhao, and L. Sun, "Switching function model-based fast-diagnostic method of open-switch faults in inverters without sensors," *IEEE Trans. Power Electron.*, vol. 26, no. 1, pp. 119–126, Jan. 2011.
[19] N. M. A. Freire, J. O. Estima, and A. J. M. Cardoso, "A voltage-based approach without extra hardware for open-circuit fault diagnosis in closed-loop PWM AC regenerative drives," *IEEE Trans. Ind. Electron.*, vol. 61, no. 9, pp. 4960–4970, Sep. 2014.
[20] N. M. A. Freire, J. O. Estima, and A. J. M. Cardoso, "Open-circuit fault diagnosis in PMSG drives for wind turbine applications," *IEEE Trans. Ind. Electron.*, vol. 60, no. 9, pp. 3957–3967, Sep. 2013.
[21] D. Diallo, M. E. H. Benbouzid, D. Hamad, and X. Pierre, "Fault detection and diagnosis in an induction machine drive: A pattern recognition approach based on concordia stator mean current vector," *IEEE Trans. Energy Convers.*, vol. 20, no. 3, pp. 512–519, Sep. 2005.
[22] D. U. Campos-Delgado, J. A. Pecina-Sánchez, D. R. Espinoza-Trejo, and E. R. Arce-Santana, "Diagnosis of open-switch faults in variable speed drives by stator current analysis and pattern recognition," *IET Electric Power Appl.*, vol. 7, no. 6, pp. 509–522, Jul. 2013.
[23] J. Zhang, J. Zhao, D. Zhou, and C. Huang, "High-performance fault diagnosis in PWM voltage-source inverters for vector-controlled induction motor drives," *IEEE Trans. Power Electron.*, vol. 29, no. 11, pp. 6087–6099, Nov. 2014.
[24] F. Wu and J. Zhao, "A real-time multiple open-circuit fault diagnosis method in Voltage-Source-Inverter fed vector controlled drives," *IEEE Trans. Power Electron.*, vol. 31, no. 2, pp. 1425–1437, Feb. 2016.
[25] J. O. Estima and A. J. M. Cardoso, "A new approach for real-time multiple open-circuit fault diagnosis in voltage-source inverters," *IEEE Trans. Ind. Appl.*, vol. 47, no. 6, pp. 2487–2494, Nov. 2011.

[26] J. O. Estima and A. J. M. Cardoso, "A new algorithm for real-time multiple open-circuit fault diagnosis in voltage-fed PWM motor drives by the reference current errors," *IEEE Trans. Ind. Electron.*, vol. 60, no. 8, pp. 3496–3505, Aug. 2013.
[27] F. Wu, Y. Hao, J. Zhao, and Y. Liu, "Current similarity based open-circuit fault diagnosis for induction motor drives with discrete wavelet transform," *Microelectron. Rel.*, vol. 75, pp. 309–316, Aug. 2017.
[28] H. Wei, Y. Zhang, L. Yu, M. Zhang, and K. Teffah, "A new diagnostic algorithm for multiple IGBTs open circuit faults by the phase currents for power inverter in electric vehicles," *Energies*, vol. 11, no. 6, p. 1508, Jun. 2018.
[29] S. Lu, W. Ye, Y. Xue, Y. Tang, and M. Guo, "Dynamic feature information extraction using the special empirical mode decomposition entropy value and index energy," *Energy*, vol. 193, Feb. 2020, Art. no. 116610.
[30] A. H. Sayed, *Fundamentals of Adaptive Filtering*. Hoboken, NJ, USA: Wiley, 2003.
[31] N. E. Huang, Z. Shen, S. R. Long, M. C. Wu, H. H. Shih, Q. Zheng, N.-C. Yen, C. C. Tung, and H. H. Liu, "The empirical mode decomposition and the Hilbert spectrum for nonlinear and non-stationary time series analysis," *Proc. Roy. Soc. London. Ser. A, Math., Phys. Eng. Sci.*, vol. 454, no. 1971, pp. 903–995, Mar. 1998.
[32] C. E. Shannon, "A mathematical theory of communication," *Bell Syst. Tech. J.*, vol. 27, no. 3, pp. 379–423, 1948.
[33] W. Sleszynski, J. Nieznanski, and A. Cichowski, "Open-transistor fault diagnostics in voltage-source inverters by analyzing the load currents," *IEEE Trans. Ind. Electron.*, vol. 56, no. 11, pp. 4681–4688, Nov. 2009.
[34] S. Abramik, W. Sleszynski, J. Nieznanski, and H. Piquet, "A diagnostic method for on-line fault detection and localization in VSI-Fed AC drives," in *Proc. 10th Eur. Conf. Power Electron. Appl. (EPE)*, 2003.

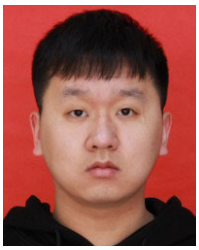

YUE WU is currently pursuing the Ph.D. degree in electrical engineering with the Shenyang University of Technology. His research interest includes multi-phase permanent-magnet machines and drives.

ZHIFENG ZHANG (Member, IEEE) was born in Huludao, Liaoning, China. He received the B.Eng. degree in automation, the M.S. degree in power electronics and power drives, and the Ph.D. degree in electrical machines and apparatus from the Shenyang University of Technology, Shenyang, China, in 2004, 2007, and 2011, respectively.

He is currently an Associate Professor with the School of Electrical Engineering, Shenyang University of Technology. His research interest includes multi-phase permanent-magnet machines and drives.

YANG LI received the master's degree in electrical engineering from the Shenyang University of Technology. Her research interest includes multi-phase permanent-magnet machines and drives.

QUANZENG SUN is currently pursuing the Ph.D. degree in electrical engineering with the Shenyang University of Technology. His research interest includes multi-phase permanent-magnet synchronous motor control.